(Received 4 July 2024, Accepted 29 August 2024, Scheduled 24 September 2024)

Isolation and Bandwidth Enhancement of Compact Wideband MIMO for Sub-6 GHz, Ku-band and Millimeter-Wave with UWB Applications

Kudumu V. Prasad[1], Narala Venkateswari[2], Miryala Sandhyarani[3], Padarti V. Kumar[4], and Kesana Mohana Lakshmi[5]

[1]*ECE, V R Siddhartha Engineering College, Siddhartha Academy of Higher Education, Vijayawada, India*
[2]*AT & T, Hyderabad, India*
[3]*ECE, Malla Reddy College of Engineering, Telangana, India*
[4]*ECE, Aditya University, Surampalem, Kakinada, India*
[5]*ECE, CMR Technical Campus, Hyderabad, Telangana, India*

ABSTRACT: A compact UWB-MIMO antenna designed for sub-6 GHz, Ku-band, and millimeter-wave applications with UWB capabilities is proposed. The antenna design consists of two inverted L-shaped MIMO elements with slot etching, deliberately positioned on an FR-4 material substrate, measuring $36 \times 18 \times 1.6\,\text{mm}^3$. Utilizing inverted L-shaped elements and prudently arranged slots on the substrate, the design achieves wideband characteristics. For enhanced isolation, interconnected rectangular slots with a fork shape are etched in the bottom layer, ensuring the isolation of less than -25 dB between ports. The proposed design exhibits an impedance bandwidth of approximately 54% within the frequency range of 3 GHz to 40 GHz, making it suitable for sub-6 GHz 5G bands, Ku-band, and millimeter-wave applications. The advantages of compactness and low profile of the proposed design are best suitable for 5G, Ku-band, and millimeter applications with UWB capabilities. The proposed design is successfully fabricated and tested.

1. INTRODUCTION

The increasing need for elevated data speeds and enhanced spectral efficiency in advanced wireless networks persists, driving the emergence of multiband multiple-input multiple-output (MIMO) antenna systems as a viable solution. A tri-band MIMO system operating across 5G Wi-Fi, Ku-band, and mm-wave frequencies, employing a 2×2 configuration on a Rogers-5880 substrate, is proposed in [1]. It incorporates a passive decoupling structure, consisting of thin microstrip lines placed between the elements and precisely designed to achieve below -20 dB. Simulation results are across a frequency range of 3 GHz to 40 GHz. In [2], a compact dual-polarized MIMO system tailored for sub-6 GHz 5G applications is presented, focusing on isolation enhancement. Utilizing plated through-hole technology, a stub is strategically placed diagonally between orthogonal ports. The structure utilizes a half mode to ensure minimal interport isolation, further augmented by additional patches to create an 8-element MIMO configuration. In [3], a MIMO is introduced, featuring high isolation and circular polarization tailored for 5G applications. This design achieves excellent isolation exceeding -20 dB. Circular polarization is attained with an axial ratio bandwidth (ARBW) of 100 MHz, 300 MHz, and 150 MHz centered at 1.2 GHz, 3.5 GHz, and 5.2 GHz, respectively. To ensure compactness and high isolation at L-band, three modified monopoles are extended on the bottom layer of the antenna using shorting pins with an in-built isolator into the ground plane to suppress MC between ports. Overall dimensions are $34\times38\times1.52\,\text{mm}^3$. A novel compact 4-port design tailored for 5G applications is introduced in [4]. The design features a two-arm monopole printed on a flexible substrate, from 3 GHz to 4.12 GHz. Key parameters such as MC between ports, DG, total active reflection coefficient (TARC), mean effective gain (MEG), envelope correlation coefficient (ECC), and channel capacity loss (CCL) were measured, resulting in improved performance. The recent planar MIMO designs, in [5], encompass various techniques such as defected ground structure (DGS), slot/stub, dielectric resonator antenna (DRA) , and metamaterial structures. These approaches offer a thorough investigation of how slots, partial ground structures, and decoupling mechanisms influence factors like isolation and bandwidth. In [6], an adaptable MIMO designed for 5G, WiFi-6E, X-band, partial Ku, and K-band applications, operating across a frequency range 3 GHz to 20 GHz, is introduced. This system employs a decoupling structure to achieve wide bandwidth and over 20 dB isolation with the utilization of partial ground and slots. The proposed antenna exhibits resonance from 3 to 7 GHz with a rectangular radiator, and from 8 to 15.4 GHz and 18.7 to 20 GHz with semi-circular strip lines. In [7], a compact 4-port antenna, shaped like a rhombus, is proposed for dual-band applications. This design features a common patch and a rhombus-shaped slot etched from the common radiator, achieves return loss values of -17 dB and -25.7 dB at 12.9 GHz and 16.5 GHz, respectively, along with gains of

* Corresponding author: Kudumu Vara Prasad (prasadkv@vrsiddhartha.ac.in).

9.62 dBi and 9.98 dBi. The study compares simulated and measured parameters, demonstrating the suitability of the design for wireless applications in the Ku-band.

In [8], a novel wideband, high-gain system, characterized by a circular shape formed through repeated etching of circles with a triangular insertion is proposed to enhance isolation. This design is fabricated on an FR-4 substrate with intentional positioning of slots, slits, and DGS within dimensions of $20 \times 32 \times 1.62\,\text{mm}^3$. The circular MIMO, featuring a fractal DGS, resonates at 16.903 GHz with an S_{11} of -43.82 dB and a gain of 6.25 dBi. This design is well suited notably for satellite communications, especially in downlinks. In [9], a novel ultra-wideband (UWB)-MIMO antenna, employs a compact $36 \times 36\,\text{mm}^2$ design with a fan-shaped isolator and 4 monopoles, aiming for high isolation and efficient indoor signal transmission. Utilizing U-shaped patches and rectangular DGS enables wide coverage from 2 GHz to 11.08 GHz. This design emphasizes isolation improvement and coupling current reduction. In [10], an approach is presented to enhance bandwidth and reduce mutual coupling (MC) in a single quad-port cross-slot antenna with co-polarized and dual-polarized patterns. Initially, the study analyzes the first, second, and third order modes of a antenna with a co-polarized pattern using characteristic mode analysis. By combining these modes, the antenna's electric-field null shifts to another unexcited port, effectively reducing MC between inter-elements. Additionally, short-ended bridges are introduced across the slot to adjust resonant frequencies, achieving MC < -17 dB within the frequency range of 4.83 to 5.68 GHz. In [11], a novel design is introduced, featuring a compact chair-shaped design with dual radiators and a single-layer frequency selective surface (FSS). This system is tailored for 5G operation within the sub-6 GHz band, and it is fabricated on a Rogers 4350B substrate. To enhance isolation and gain, the design incorporates both a parasitic element and an FSS array structure, comprising square-shaped cells with a circular slot, implemented using a surround technique. In [12], a novel superstrate employing FSS technology is introduced. This superstrate aims to mitigate MC between closely spaced circularly polarized radiators. The proposed design achieves a significant reduction in MC, ranging from -8.7 to -26 dB. In [13], a MIMO antenna designed to operate at 77 GHz features two columns of 12 transmitting sawtooth antenna arrays and two rows of 24 receiving sawtooth antenna arrays, arranged in a rectangular ring. Both the transmitting and receiving units incorporate a metal cavity topology powered by a substrate integrated waveguide (SIW) slot. Additionally, multiple 3×3 metal pin arrays enhance the system's gain and isolation. Simulation results show an isolation level of 42 dB across the 75–81 GHz range, with its significant gain and isolation, suitable for millimeter-wave automotive radar applications. In [14], a MIMO-UWB antenna, operating at frequencies of 2.94 GHz and 11.61 GHz, featuring a C-band notch, is proposed for wireless communication. The radiators are printed on an FR4 substrate measuring $40 \times 21\,\text{mm}^2$. The design consists of circularly notched rectangular patches embedded with ellipses. MC is reduced to below -18 dB across the 2.94–11.61 GHz bandwidth without using any coupling devices by positioning the two radiators side-by-side with a separation of $0.03\lambda_0$.

In [15], a slot-shaped EBG structure with unit cell size 6.3 mm $\times$ 6.3 mm is proposed, resonating at a 5.8 GHz frequency. As the substrate is FR-4 epoxy, the effect of surface waves in patch arrays is predominant. The use of the proposed design will adapt the $S_{11} < -10$ dB and $S_{12} < -51$ dB and avoid surface waves. Slots are used to change the current distribution, and the design is implemented for WLAN application. In [16], a MIMO antenna is proposed for achieving quasi-omnidirectional circular polarization, intended for the integration of sensing and communications of 6G technology. This architecture is composed of three dielectric laminates stacked one above or below the other, with each substrate positioned adjacent to its counterpart separated by an air cavity. On the top and bottom of the middle substrate, impedance matching transmission lines and reactive impedance surfaces are printed, respectively. The antenna occupies a footprint of $1.2\lambda \times 1.2\lambda$ and has a height of 0.1λ at 12 GHz, aiming to demonstrate quasi-omnidirectional circular polarization (OCP). In [17], a tri-band MIMO design is introduced for 5G/WIFI 6E wearable applications, featuring a rectangular monopole etched with an inverted U-shape slot and an L-shape branch. The design operates across three frequency bands: 2.54–3.56 GHz, 4.28–4.97 GHz, and 5.37–8.85 GHz and is fabricated on a Liquid Crystal Polymer substrate measuring $56 \times 56 \times 0.1\,\text{mm}^3$. Improved isolation exceeding 20 dB is achieved by integrating a crossed branch with two circular rings. In [18], a comprehensive review of multiband MIMO designs tailored for wireless applications in 5G and 6G is outlined. The review aims the necessity of MIMO within the sub-6 GHz, to explore diverse techniques for generating multiband capabilities, to address challenges encountered in designing multiband MIMO for 5G or 6G, and to examine methods for achieving circular polarization and pattern diversity to enhance overall performance. In [19], a method for decoupling between two tri-band antennas suitable for LTE, WLAN, and 5G applications is introduced. The 3.5 GHz band is addressed with a monopole design, while adjustments to the partial ground plane enable resonance in the other two bands. Surface wave currents in the low band is mitigated by employing split ring resonators (SRRs) to counteract coupling effects. This MIMO antenna spans 2.4 GHz, 3.5 GHz, and 5.8 GHz bands, covering LTE, 5G, and WLAN, respectively. In [20], a compact MIMO-UWB antenna featuring a C-band notch is proposed for wireless applications. The design consists of a patch with circular notches, incorporating an embedded ellipse. Fabricated on an FR4 substrate measuring $40 \times 21\,\text{mm}^2$, a U-type slit is introduced to create a band-notch in the C-band, spanning 3.63–4.15 GHz. In [21], a comprehensive review of various techniques aimed at reducing MC in MIMO systems, crucial for maintaining consistent radiation patterns and polarization in telecommunications is proposed. To address MC issue, employing techniques like DGS, parasitic or slot elements, complementary SRR (CSRR), and decoupling networks proves to be a simple yet effective approach. In [22], a compact MIMO antenna optimized for robust isolation in portable UWB applications is presented. The design features two rectangular elements with narrow slots incorporated into the ground plane,

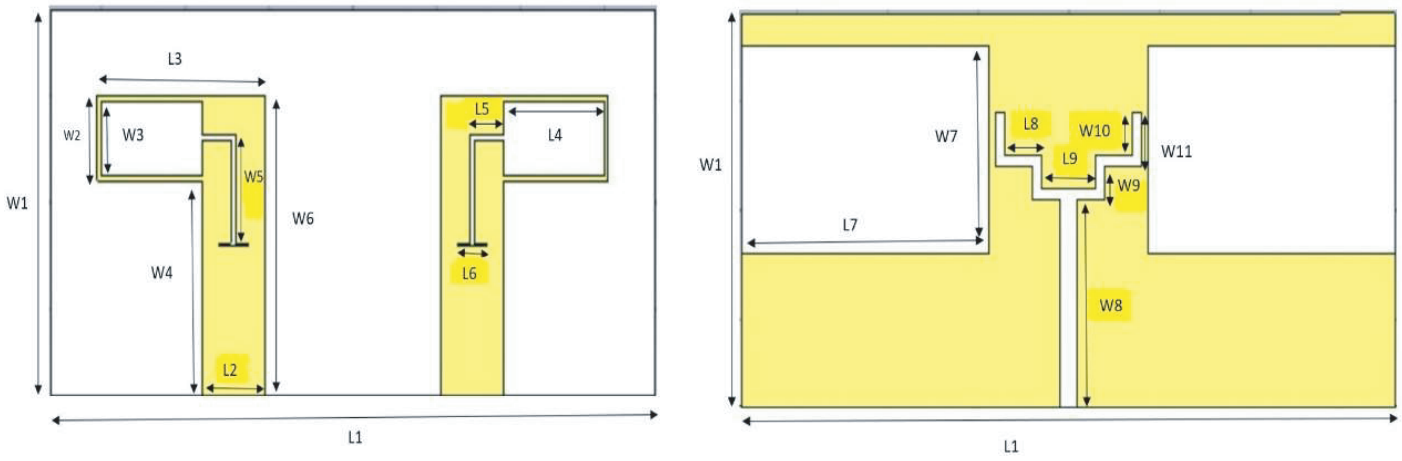

FIGURE 1. Proposed MIMO antenna design.

resulting in a bandwidth ranging from 2.1 to 16.9 GHz, encompassing the S, C, X, and Ku bands. Enhanced isolation exceeding 16 dB is achieved by integrating two inverted L-shaped stubs into the ground structure. The design, with dimensions $36 \times 38\,\text{mm}^2$, demonstrates strong performance across various MIMO metrics. In [23], a ten-element MIMO system is introduced, aiming to mitigate cross-polarization and enhance isolation in the millimeter-wave range. Each element features a stub-loaded CPW structure with an elliptical radiator. To diminish MC effects, DGS is utilized, achieved by engraving partial elliptical slots into the coplanar ground. This structural modification serves as a reflector, enhancing radiation properties and reducing cross-polarization and isolation between adjacent elements. The antenna achieves isolation levels below -35 dB across the mm spectrum for any adjacent element pair. The antenna layout spans $3.4\lambda \times 8.5\lambda$, with an inter-element spacing of 0.44λ. In [24], a dual-band antenna tailored for mm-wave frequencies of 28 and 38 GHz, envisaged for future mobile communication standards, is presented. The primary element, fed via strip line with inset feed, is accompanied by a parasitic element. The latter is fed through capacitive coupling with the main element. In [25], a MIMO antenna operating at 28/38 GHz frequencies for 5G networks is introduced. The design features slot monopole antenna elements loaded with stubs and small crescents. One antenna is printed on the upper layer, while the other is on the back of the substrate, enhancing element coupling without requiring decoupling structures. Dual-band functionality at 28/38 GHz is achieved by adjusting stub and crescent dimensions.

In [26], a 4-port MIMO system with circular polarization operating at 5.9 GHz is introduced for vehicle-to-everything (V2X) communications. To minimize MC between the elements, a hybrid decoupling structure comprising circular ring parasites and DGS is employed. In [27], a solution for mitigating MC in MIMO for WLAN applications is introduced, employing CSRR unit cells. A Vivaldi array is engineered, incorporating compact triple-band gap-CSRR unit cells between two elements to assess their impact on MC reduction. Through the integration of CSRR units, the proposed design demonstrates enhanced decoupling, achieving improvements of 8.5 dB, 10.5 dB, and 18 dB at frequencies of 3.65 GHz, 4.9 GHz, and 5.8 GHz, respectively. In [28], a two-element UWB-MIMO design featuring MC minimization is implemented using four T-shaped slots on the patch, mounted on a $50 \times 25\,\text{mm}^2$ FR-4 substrate. The reduction in MC is attained through the inclusion of a T-shaped ground stub and a slot, catering to applications such as WiMAX, WLAN, X-band SATCOM, radar, and commercial WLAN. In [29], primarily, the focus has been on microstrip feed antennas suitable for short-range communications. Various techniques have been explored, such as truncating radiating elements, employing artificial materials, and slotting both the patch and ground plane. In [30], an approach to the problem of estimating the average channel capacity assigned to each user of a spread spectrum (SS)-MIMO system operating in a Rayleigh fading environment is presented.

The literature presented in the introduction discussed numerous methods to enhance isolation. The design proposed in this article is a simple-miniaturized design with the utilization of inverted L-shaped elements and prudently arranged slots on the substrate, and the design achieves wideband characteristics from 3 GHz to 40 GHz. For enhanced isolation, interconnected rectangular slots with a fork shape stub is etched in the bottom layer, ensuring the isolation of less than -25 dB between ports. A comparison table is presented in Section 5.

The article is organized in the prescribed steps. The proposed design with different parameter analysis is explained in Section 2. Section 3 presents the result analysis of the design in this article. Simulation and measurement results are explained in Section 3. Section 4 presents the analysis of the MIMO design and MIMO parameter analysis of the design. Finally, Section 5 presents the conclusion.

2. DESIGN METHODOLOGY

A two-port MIMO antenna has been designed, simulated, and fabricated on an FR4 substrate. The geometry (front and back views) of the proposed antenna is shown in Fig. 1, with the optimal design parameters detailed in Table 1. To achieve excellent isolation, a decoupling structure which consists of in-

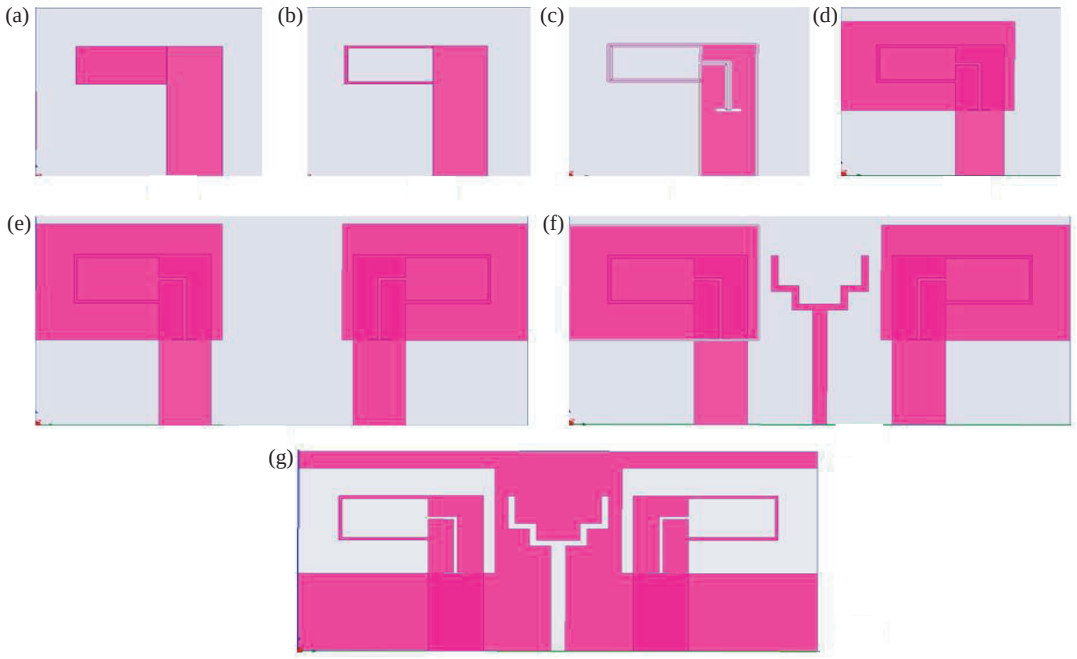

FIGURE 2. Evolution of the proposed design from (a)–(g).

TABLE 1. Optimized parameters.

Parameter	Dimension (mm)
L_1	**36**
W_1	18
L_2	3
W_2	4
L_3	10
W_3	3.5
L_4	6
W_4	10
L_5	2.02
W_5	5.04
L_6	1.7
W_6	14
L_7	13.6
W_7	9.5
L_8	2
W_8	9.5
L_9	3
W_9	1.5
W_{10}	2
W_{11}	2.5

terconnected rectangular slots with a fork shape stub is implemented on the ground plane. The design has been simulated using CST, and various MIMO antenna parameters have been analyzed. The overall dimensions of the MIMO antenna are $W1\,\text{mm} \times L1\,\text{mm}$. The evolution process is shown in Fig. 2.

Figure 2(a) shows the initial patch with two rectangular slots. In Fig. 2(b), a single rectangular slot is etched from the patch. Fig. 2(c) introduces an inverted L-shaped slot etched into the patch. A rectangular ground plane is added beneath the substrate in Fig. 2(d). Fig. 2(e) displays a mirror image of the design. In Fig. 2(f), a decoupling structure which consists of interconnected rectangular slots with a fork shape stub is added to achieve wide bandwidth and improved isolation. The final design is presented in Fig. 2(g).

2.1. Two-Port Antenna Design

The two antennas are positioned adjacent to each other on the top layer of the substrate, with element-2 being a mirror image of element-1, as shown in Fig. 1. The overall design dimensions are $18\,\text{mm} \times 30\,\text{mm} \times 1.6\,\text{mm}$. The edge-to-edge spacing between the two adjacent elements is 10.4 mm, and the port width is 3 mm. The structure is designed using these optimal dimensions to achieve wide bandwidth and excellent isolation. The evolution of the proposed MIMO system is illustrated in Fig. 2, detailing each step. Fig. 3 displays the S-parameter analysis, indicating that S_{11} is below $-10\,\text{dB}$, reflecting frequencies from 4 GHz to 40 GHz. Furthermore, S_{12} is below $-25\,\text{dB}$, showcasing excellent port isolation. To enhance isolation further, modifications are made to the ground plane, as depicted in Fig. 2, incorporating C-inverted C slots and a decoupling structure which is interconnected rectangular slots with a fork shape stub. Final step of the design achieves notable improvements in isolation and impedance bandwidth.

3. RESULTS AND DISCUSSION

The depicted two-port MIMO design has been fabricated, with S-parameters measured using a vector network analyzer and

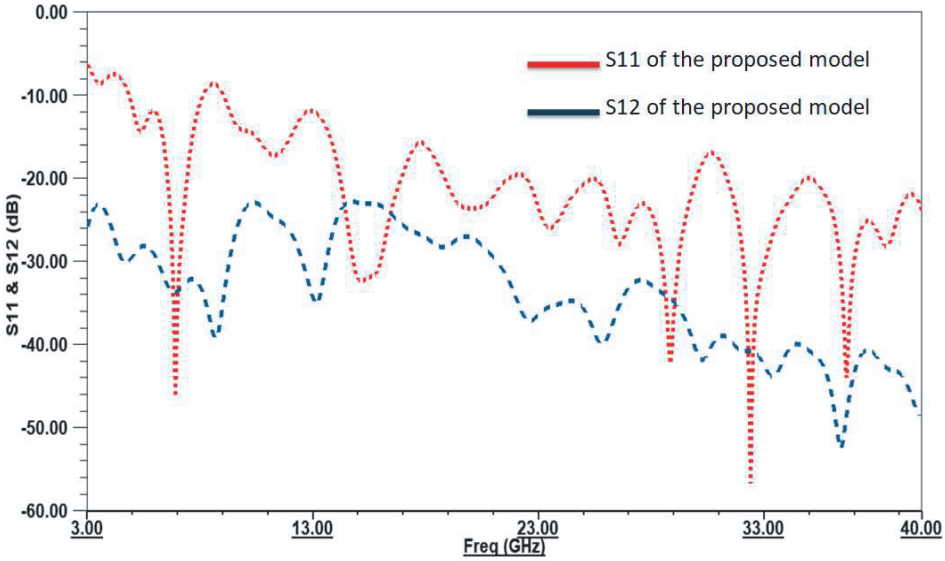

FIGURE 3. Simulated S_1 and S_{12} of the design proposed.

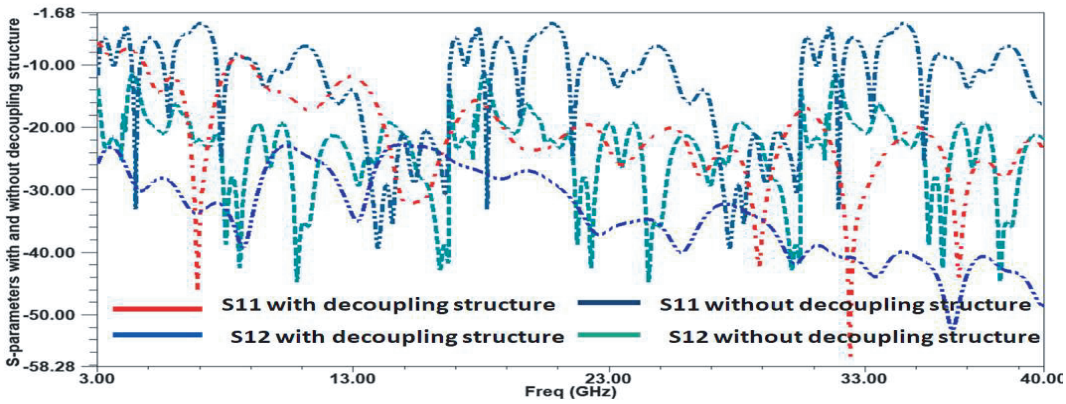

FIGURE 4. S-parameters with and without decoupling structure.

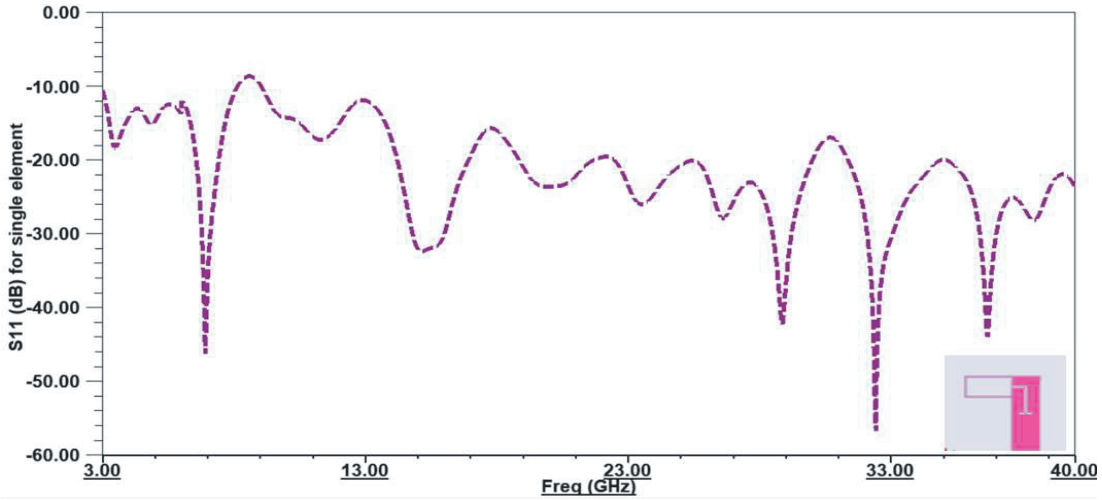

FIGURE 5. Simulated S_{11} for the single element.

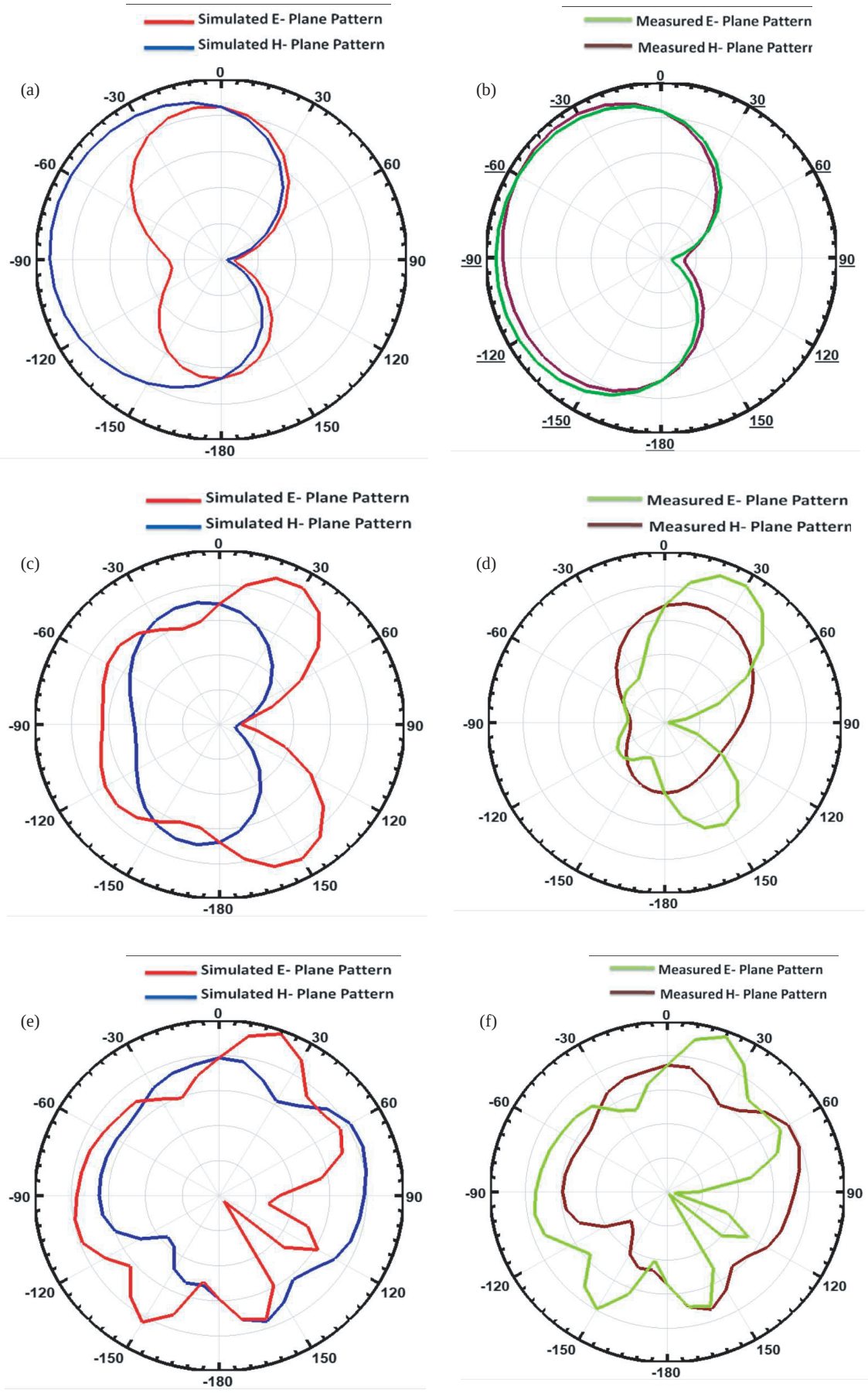
Simulated E- Plane Pattern
Simulated H- Plane Pattern
(a)
Measured E- Plane Pattern
Measured H- Plane Pattern
(b)
Simulated E- Plane Pattern
Simulated H- Plane Pattern
(c)
Measured E- Plane Pattern
Measured H- Plane Pattern
(d)
Simulated E- Plane Pattern
Simulated H- Plane Pattern
(e)
Measured E- Plane Pattern
Measured H- Plane Pattern
(f)
0
30
60
90
120
150
-180
-150
-120
-90
-60
-30

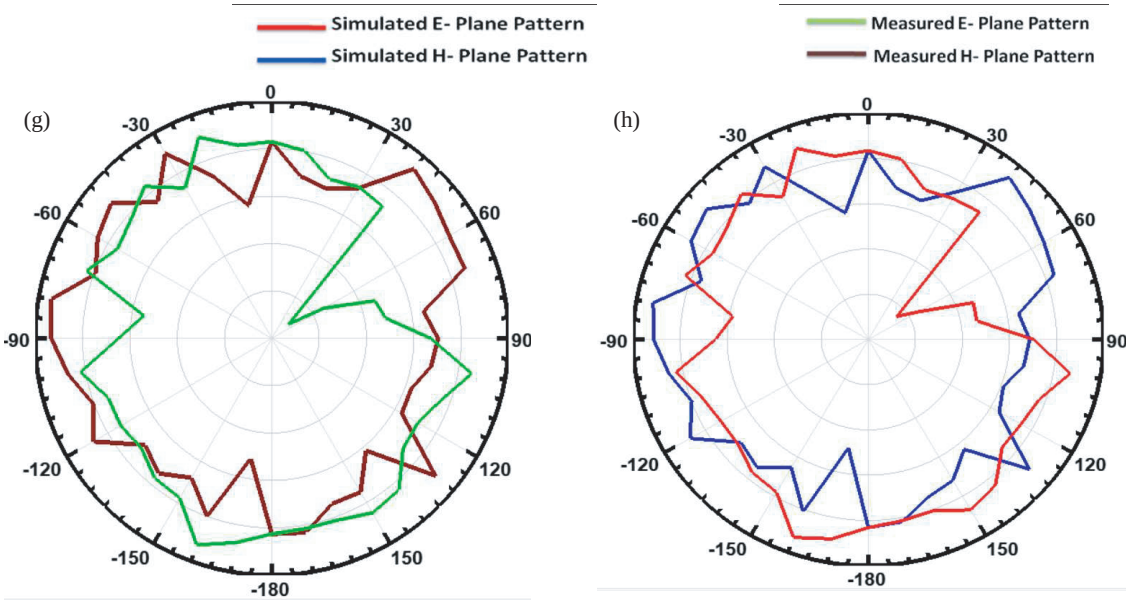

FIGURE 6. Radiation patterns of the design. (a) Simulated E-plane and H-plane pattern at 3 GHz. (b) Measured E-plane and H-plane pattern at 3 GHz. (c) simulated E-plane and H-plane pattern at 5.8 GHz. (d) measured E-plane and H-plane pattern at 5.8 GHz. (e) Simulated E-plane and H-plane pattern at 15 GHz. (f) Measured E-plane and H-plane pattern at 15 GHz. (g) Simulated E-plane and H-plane pattern at 38 GHz. (h) Measured E-plane and H-plane pattern at 38 GHz.

radiation patterns observed in an anechoic chamber. The simulated S_{11} and S_{12} results for the proposed design are illustrated in Fig. 3. It can be observed that the simulated S_{11} for the proposed design is < 10 dB throughout the frequency range 3 GHz to 40 GHz.

Figure 4 shows the S-parameters with and without the decoupling structure. Without the structure, S_{11} and S_{12} are around -10 dB and -20 dB, respectively. With the structure integrated into the design, S_{11} and S_{12} fall below -15 dB and -25 dB across the band from 3 GHz to 40 GHz. This improvement is attributed to the mitigation of surface currents by the decoupling structure. Specifically, the defected ground with C-inverted C slots and a decoupling structure which is interconnected rectangular slots with a fork shape stub effectively reduces surface currents in the substrate, thereby decreasing the mutual coupling between elements.

Figure 5 depicts the S_{11} parameter for the single element. S_{11} is below -10 dB for the entire band of frequencies 3 GHz to 40 GHz. The modeling of the proposed structure is analyzed using two rectangular patches on top side of the substrate. The stripline dimensions are 10×3 mm^2. Next, from the horizontal patch, we remove a portion of the rectangular slot, as shown in Figs. 2(b) and 2(c), for better impedance bandwidth and etch an inverted L-shaped structure to the vertical rectangular slot, which results in a better S_{11}, which is < -10 dB.

Lastly, an inverted C-shaped ground is provided, which leads to wideband characteristics. All these steps are depicted in Fig. 2. The proposed single-element design incorporates three distinct steps: The inclusion of a slotted-shape radiator on the front side and a defected ground on the back side, effectively operating from 3 to 40 GHz. The use of a partial ground, with a decoupling structure contributes to a wide impedance bandwidth, and provides high isolation. The partial ground, with a decoupling structure which consists of interconnected rectangular slots with a fork shape stub developed on the bottom side of the substrate, contributes to improved isolation improved isolation between elements while simultaneously improving impedance matching.

The simulated and measured radiation patterns are depicted in Fig. 6, with the help of an anechoic chamber, which can measure up to 40 GHz frequency. Port-1 of the radiating element was excited. Fig. 6 relates the simulation results with the measured radiation pattern. For 3 GHz, a peak gain of 3.05 dB is presented in Fig. 6(a). For 5.8 GHz, the peak gain of 3.7 dB is shown in Fig. 6(c). Also, for 15 GHz the maximum gain of 6.3 dB was observed and presented in Fig. 6(e). Finally, the peak gain of 2.9 dB is achieved at 38 GHz and depicted in Fig. 6(g).

Figure 7 illustrates the surface current distributions, emphasizing the crucial role of the decoupling structure in enhancing the isolation between elements. The decoupling networks equivalent representation is composed of capacitors and inductors strategically positioned between the antenna elements, and tuned to achieve optimal isolation. These networks help reduce the coupling between adjacent antennas, ensuring that signals transmitted or received by one element minimally affect the others.

The fabricated two-port proposed design is shown in Figs. 8(a) and 8(b). Measurements were conducted using a Keysight (model N9916A) Vector Network Analyzer (VNA), and the radiation pattern was assessed in an anechoic chamber. The simulated and measured S_{11} and S_{12} parameters are presented in Fig. 10. Fig. 9 illustrates the measurement environment for the proposed design.

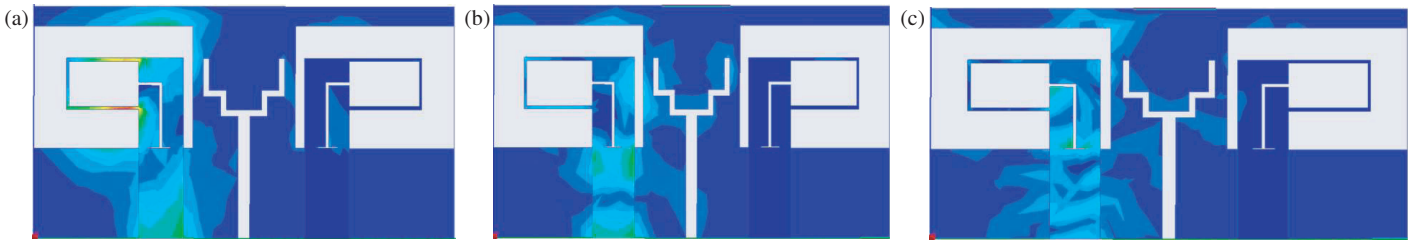

FIGURE 7. Surface current distribution (J) of the MIMO antenna at frequencies. (a) 5.8 GHz. (b) 15 GHz. (c) 30 GHz.

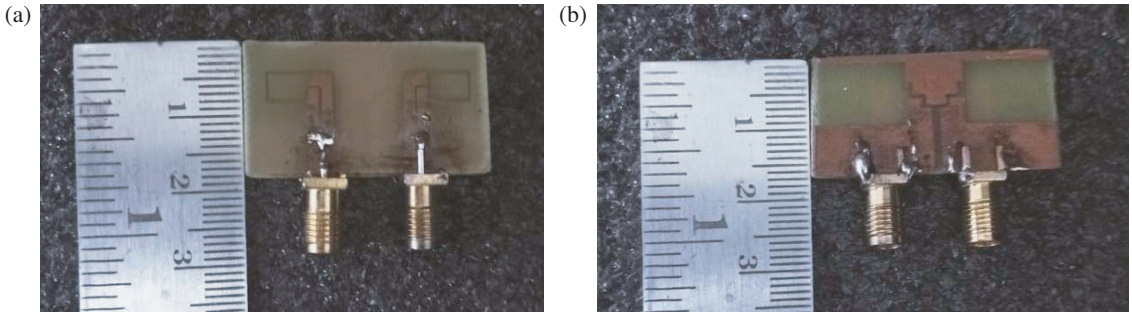

FIGURE 8. Fabricated MIMO design. (a) Front view. (b) Rear view.

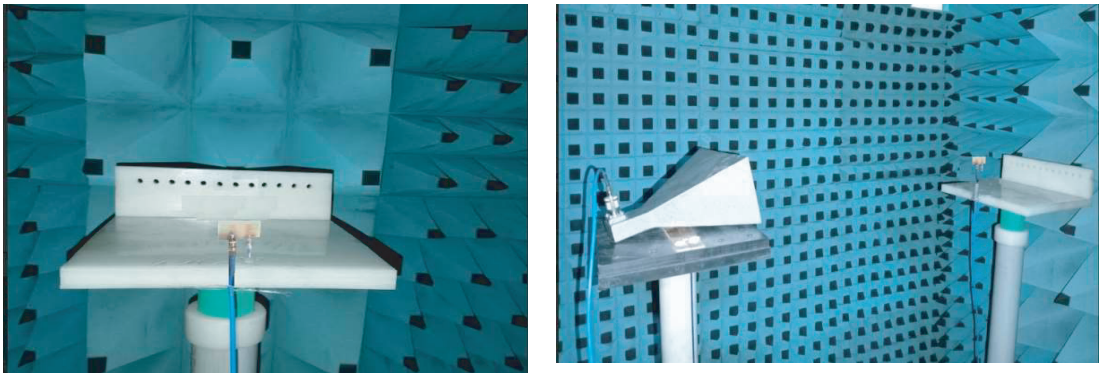

FIGURE 9. Proposed design measurement setup in an anechoic chamber.

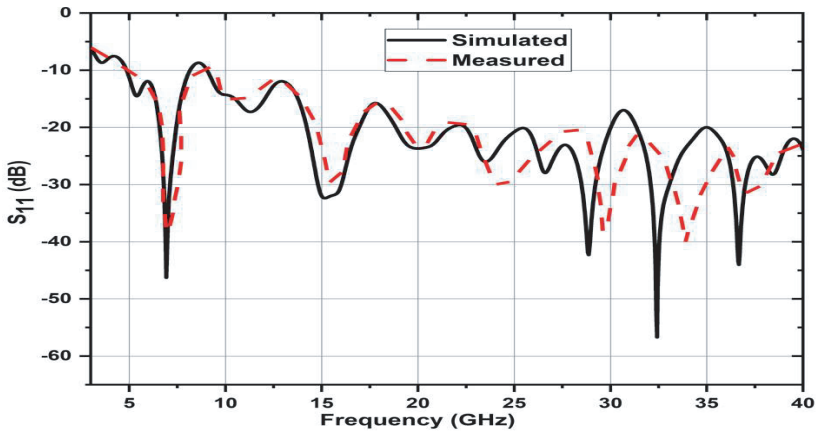

FIGURE 10. Simulated and measured S_{11} for the design proposed.

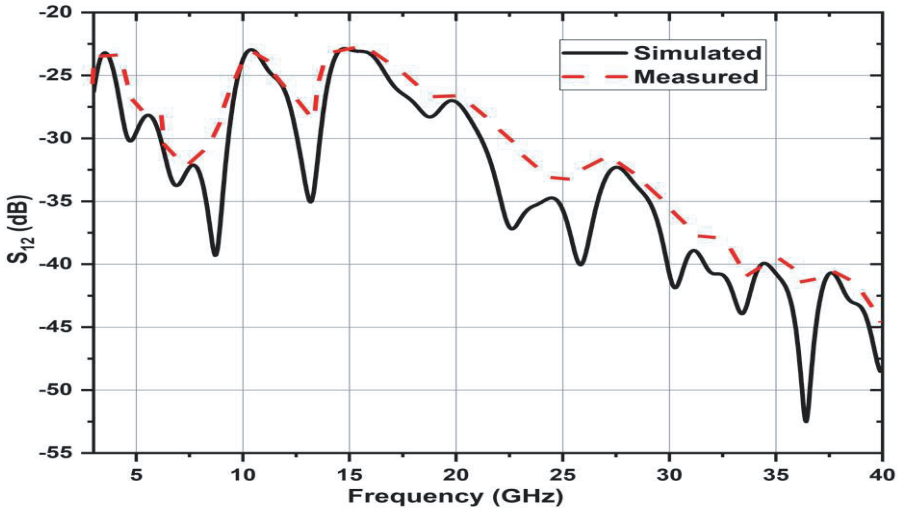

FIGURE 11. Simulated and measured S_{12} for the design proposed.

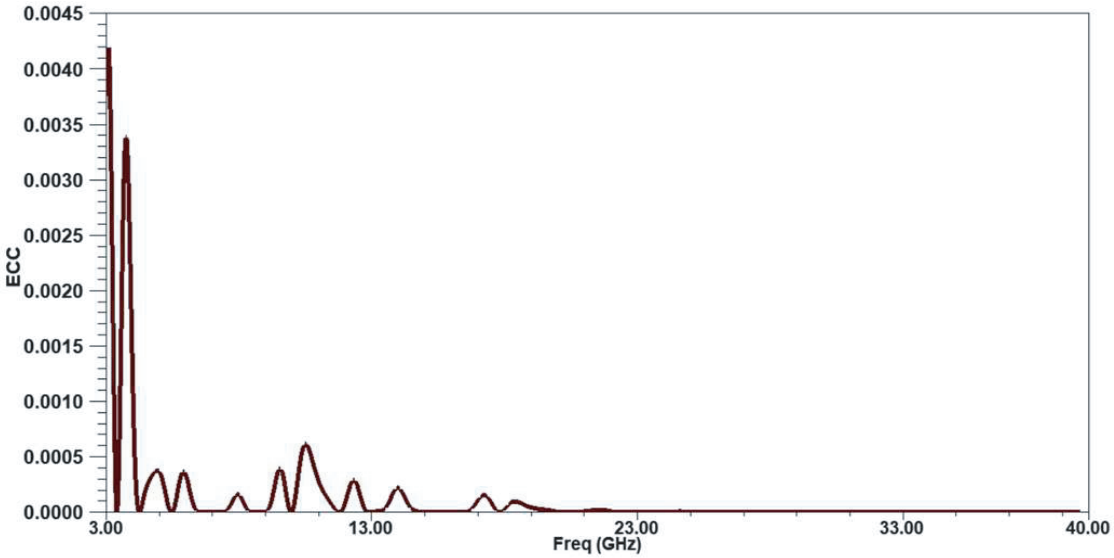

FIGURE 12. Envelope Correlation Co-efficient (ECC) for the proposed design.

Fig. 10 and Fig. 11 clearly depict that the simulated and measured S_{11} and S_{12} results are slightly mismatched due to fabrication tolerances, and better impedance bandwidth (IBW) is achieved throughout the frequency band of 3.1 GHz to 40 GHz.

4. MIMO PARAMETERS PLOTS FOR THE PROPOSED DESIGN

The validation of the proposed design involves computing MIMO parameters such as ECC, DG, TARC, and MEG. ECC computation analysis is performed using S-parameters as referenced in [28], and the ECC is less than 0.05, as illustrated in Fig. 12. Fig. 13 shows a DG of 9.9 dB. The ECC, based on S_{12}, is described by field-based Equation (1), in terms of Θ and ϕ, and specifies the correlation patterns between the two radiating elements.

$$\rho_e = \frac{\left|\int_0^{2\pi}\int_0^{\pi}\left(XPR\cdot E_{\theta 1}\cdot E_{\theta 2}^{*}\cdot P_{\theta}+E_{\varphi 1}\cdot E_{\varphi 2}^{*}\cdot P_{\varphi}\right)d\Omega\right|}{\int_0^{2\pi}\int_0^{\pi}\left(XPR\cdot E_{\theta 1}\cdot E_{\theta 2}^{*}\cdot P_{\theta}+E_{\varphi 1}\cdot E_{\varphi 2}^{*}\cdot P_{\varphi}\right)d\Omega \times \int_0^{2\pi}\int_0^{\pi}\left(XPR\cdot E_{\theta 1}\cdot E_{\theta 2}^{*}\cdot P_{\theta}+E_{\varphi 1}\cdot E_{\varphi 2}^{*}\cdot P_{\varphi}\right)d\Omega} \quad (1)$$

DG represents the reduction in the required receiving signal-to-noise ratio (SNR) for a given bit error rate (BER), averaged over fading conditions. It specifically measures the decrease in fading margin obtained by minimizing the effects of fading with the MIMO antenna. This indicates good diversity performance and demonstrates excellent results within the proposed frequency band. DG is the ratio of rise in mixed signals SNR from multiple elements to the SNR from a single element in the MIMO system. DG [3] is related to ECC and can be expressed

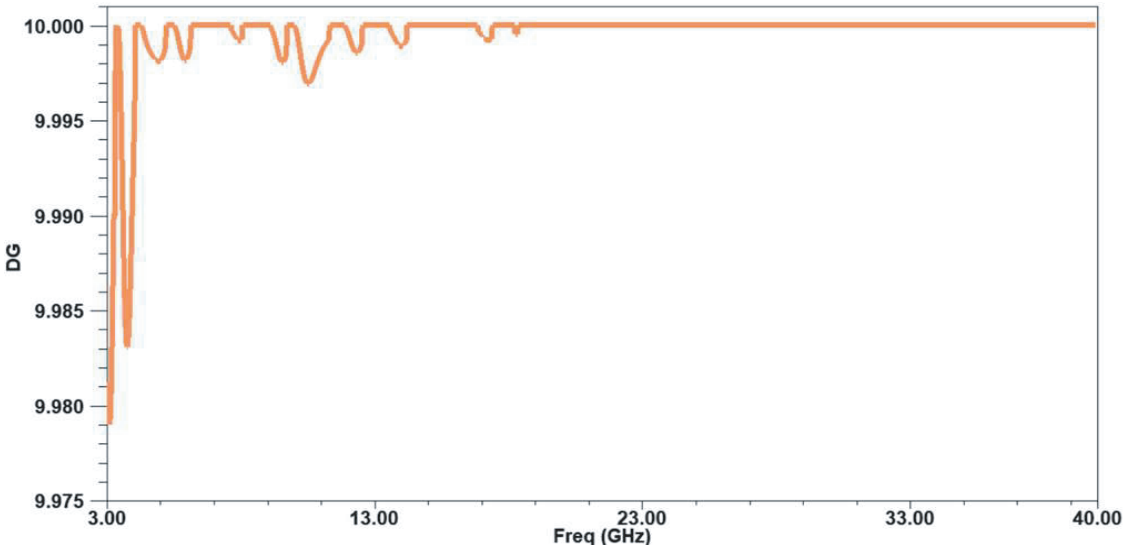

FIGURE 13. Diversity Gain (DG) for the proposed design.

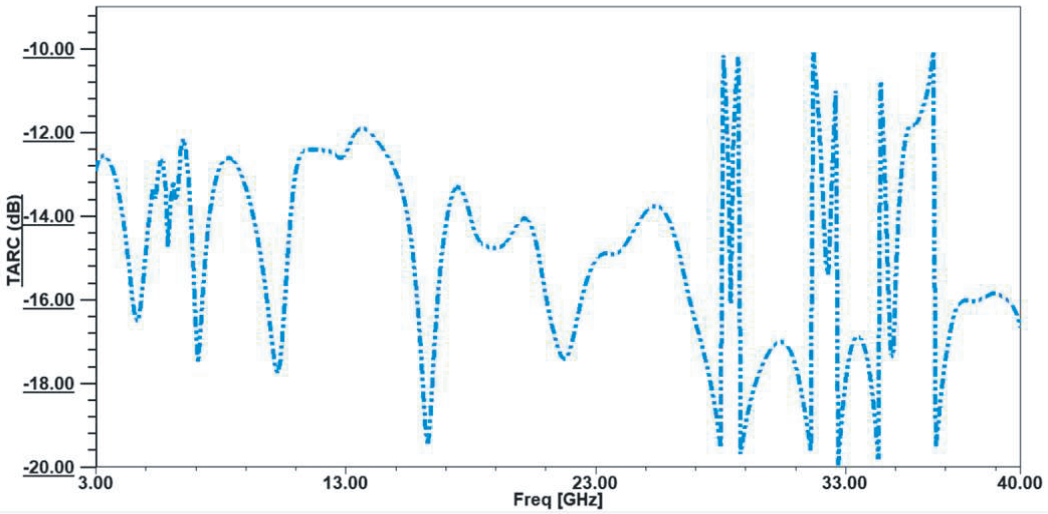

FIGURE 14. Total Active Reflection Co-efficient (TARC) for the proposed design.

as follows:

$$DG = 10\sqrt{1 - ECC} \tag{2}$$

TARC relates the total incident power to the total outgoing power in an N-port antenna system and is a function of frequency. It is primarily used for MIMO antenna systems, where the outgoing power is the undesired reflected power. TARC is calculated as the square root of the sum of all outgoing powers at the ports divided by the sum of all incident powers at the ports of an N-port antenna. It can be directly computed from the scattering matrix and is expressed in Equation (3) [6],

$$\Gamma_a^t = \frac{\sqrt{\sum_{i=1}^{N} |b_i|^2}}{\sqrt{\sum_{i=1}^{N} |a_i|^2}} \tag{3}$$

where a_i represents an incident wave, and b_i denotes a reflected wave. As shown in Fig. 14, the TARC for the proposed frequency band is lower than -10 dB.

CCL is another critical diversity parameter which describes the highest attainable limit of communication transmission rate. CCL is depicted in Fig. 15 [6], and it is observed that the CCL is under 0.4 bits/s/Hz.

$$\begin{aligned} C_{loss} &= -\log_2 \det\left(\alpha^R\right) \\ where, \quad \alpha^R &= \begin{bmatrix} \alpha_{11} & \dots & \alpha_{14} \\ \vdots & \ddots & \vdots \\ \alpha_{41} & \dots & \alpha_{44} \end{bmatrix} \\ and \quad \alpha_{ii} &= 1 - \left(\sum_{j=1}^{N} |S_{ij}|^2\right) \\ Also \quad \alpha_{ii} &= -\left(S_{ij}^* S_{ij} + S_{ji}^* S_{ij}\right) \end{aligned} \tag{4}$$

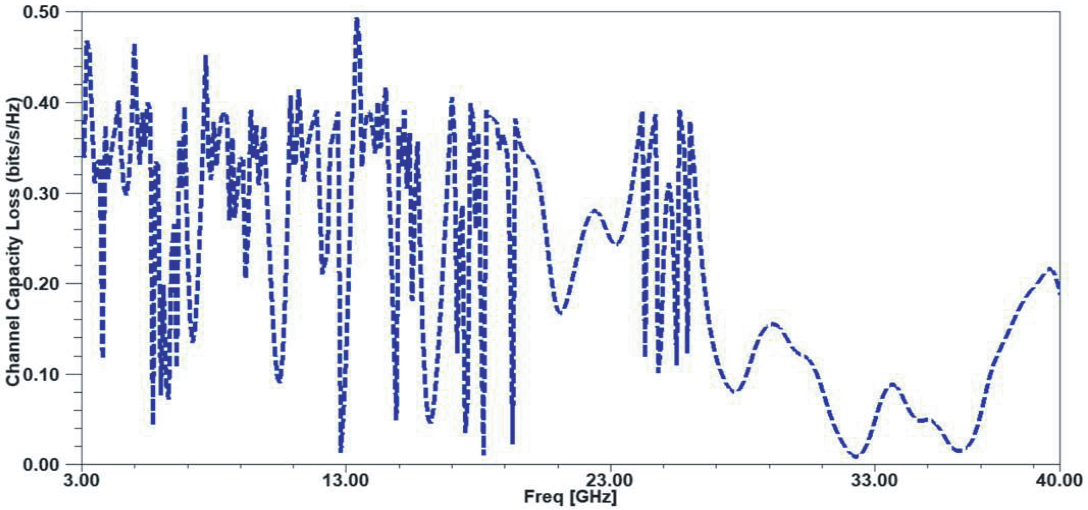

FIGURE 15. Channel capacity loss (CCL) for the proposed design.

TABLE 2. Comparative analysis between the proposed design and the literature designs.

Ref.	MIMO designsize (mm^3)	Frequency of operation (GHz)	Isolation Technique	S_{11} & S_{12} (in dB)	Peak Gain (dBi)	ECC & DG	Spacing between Elements	Design Complexity	Substrate Used
[6]	$29\times28\times1.6$	3.0–7.0, 8.0–15.4 & 18.7–20	Defective slotted ground	<-10 & <15	6.23	<0.006 & >9.99	18	Simple	FR-4
[8]	$20\times32\times1.6$	16.9	Fractal DGS	-43.82 & <-15	6.25	<0.025 & >9.89	16	Simple & Implemented for Satellite Communication	FR-4
[15]	$52\times30\times1.6$	5.8	EBG	<-16 & <-48	-	-	30.6	Simple	FR-4
[17]	$56\times56\times0.1$	2.54–3.56, 4.28–4.97 and 5.37–8.85	Inverted U-Shape slot and a L-Shape branch and loading a Crossed branch with two circular rings	<-10 & 20	1.8, 2.6 and 3.2	<0.13 & 9.95	-	Flexible	LCP
[20]	$21\times40\times1.6$	2–18	UWB-MIMO with U-slot	<-10 & <-20	4.21	<0.002 & 9.999	3.06	Simple	FR-4
[22]	$36\times38\times1.6$	2.1–16.9	L-shaped stubs in the ground plane	<-10 & <-16	3	<0.018 & >9.96	18.15	Simple	FR-4
[24]	$26\times26\times0.25$	28 & 38	Parasitic element	<-20 & <-40	7.37 & 8.13	<0.0005 & >9.99	-	Complex	Rogers RO3003
[25]	$30\times15\times1.6$	28 & 38	Stub	<-10 & -36.7	5.7 & 6.9	<0.0001 & >9.999	-	Simple	Rogers RO3003
[28]	$25\times50\times1.6$	3.1–12	T-stub and Ground Slot	<-10 & <-15	4.95	<0.05 & >9.99	10.75	Simple	FR-4
Prop.	**$36\times18\times1.6$**	**3-40**	**Defected slotted ground with slotted patch**	<-10 & <-20	**3.05 dB at 3 GHz, 3.7 dB at 5.8 GHz, 6.3 dB at 15 GHz, 2.9 dB at 38 GHz**	**<0.0005 & >9.999**	**10.4**	**Simple**	**FR-4**

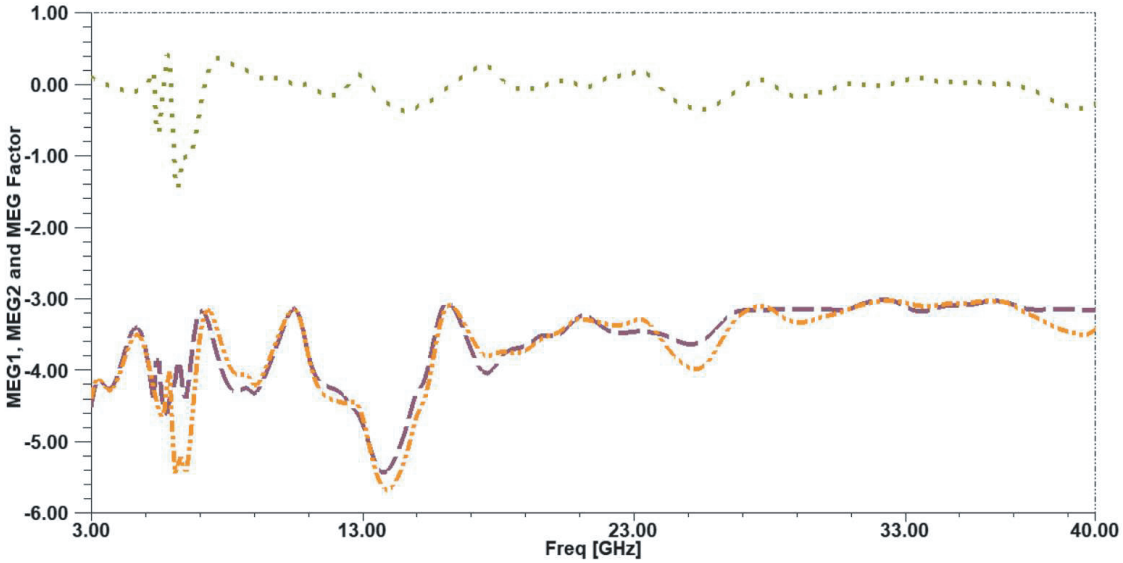

FIGURE 16. Mean Effective Gain (MEG) for the proposed design.

Mean effective gain (MEG) represents the power received by a diversity antenna compared to the power received by an isotropic radiator, calculated using Equation (5) [1]. The MEG ratio, k, indicates the power ratio between MEG1 and MEG2, which must be less than 3 dB.

Figure 16 displays the plots of MEGs and power ratio k for the proposed design, showing that k remains below 3 dB.

$$MEG_i = 0.5\mu_{i,rad} = 0.5\left(1 - \sum_{j-1}^{M} |S_{ij}|\right) \tag{5}$$

Table 2 provides a comparison between the proposed design and other designs provided in the literature. This comparison indicates that the proposed design is extremely simple and inexpensive compared with other designs, as discussed in the literature in terms of IBW, isolation, size, ECC, and DG.

5. CONCLUSION

A compact UWB-MIMO antenna designed for sub-6 GHz, Ku-band, and millimeter-wave applications with ultra-wideband (UWB) capabilities has been simulated, fabricated, and tested. The design features two inverted L-shaped MIMO elements with slots etching on an FR-4 substrate. By incorporating inverted L-shaped elements and strategically arranging slots on the substrate, the design achieves wideband characteristics with $S_{11} < -10$ dB and enhanced isolation, $S_{12} < -25$ dB between ports across the operating band. The proposed design demonstrates an impedance bandwidth of approximately 54% within the frequency range of 3 GHz to 40 GHz, making it suitable for sub-6 GHz 5G bands, Ku-band, and millimeter-wave applications. The MIMO parameters, including ECC, DG, TARC, CCL, and MEG, are simulated and fall within acceptable limits. The compact and low-profile nature of the proposed design makes it ideal for 5G, Ku-band, and millimeter-wave applications with UWB capabilities. The proposed design has been successfully fabricated and tested.

REFERENCES

[1] Ali, A., M. E. Munir, M. M. Nasralla, M. A. Esmail, A. J. A. Al-Gburi, and F. A. Bhatti, "Design process of a compact tri-band MIMO antenna with wideband characteristics for sub-6 GHz, Ku-band, and millimeter-wave applications," *Ain Shams Engineering Journal*, Vol. 15, No. 3, 102579, 2024.

[2] Cholavendan, M. and V. Rajeshkumar, "Dual-feed orthogonally polarized compact 8-element MIMO antenna using metallic stub and decoupling unit for isolation enhancement of sub-6 GHz 5G application," *Progress In Electromagnetics Research Letters*, Vol. 116, 105–111, 2024.

[3] Sharma, U., G. Srivastava, M. K. Khandelwal, and R. Roges, "Shorting pins-based triple band circularly polarized modified monopole compact dual-port MIMO antenna for sub-6 GHz wireless applications," *AEU — International Journal of Electronics and Communications*, Vol. 176, 155162, 2024.

[4] Abdelghany, M. A., A. A. Ibrahim, H. A. Mohamed, and E. Tammam, "Compact sub-6 GHz four-element flexible antenna for 5G applications," *Electronics*, Vol. 13, No. 3, 537, Jan. 2024.

[5] Aggarwal, R., A. Roy, and R. Kumar, "Millimeter wave antennas: A state-of-the-art survey of recent developments, principles, and applications," *Progress In Electromagnetics Research B*, Vol. 104, 147–169, 2024.

[6] Ali, A., M. Rasool, M. Z. Zahid, I. Rashid, A. M. Siddique, M. Maqsood, and F. A. Bhatti, "A 4-port broadband high-isolated MIMO antenna for wireless communication," *Progress In Electromagnetics Research C*, Vol. 142, 119–130, 2024.

[7] Phaneendra, C. N. and K. K. Naik, "Design of dual band MIMO antenna with rhombus shape for wireless applications," *Progress In Electromagnetics Research M*, Vol. 124, 63–70, 2024.

[8] Sanugomula, M. and K. K. Naik, "A compact high gain circular shaped two-port MIMO antenna with fractal DGS for downlink satellite communication," *Progress In Electromagnetics Research M*, Vol. 125, 135–142, 2024.

[9] Ren, W., Z.-G. Wang, M. Yang, J. Zhou, and W.-Y. Nie, "Design of a simple four-port UWB-MIMO antenna based on a fan-shaped isolator," *Progress In Electromagnetics Research M*, Vol. 126, 117–126, 2024.

[10] Liu, N.-W., J.-L. Fan, L. Zhu, Q. Wu, Y. Liu, and S. Sun, "Mutual-coupling reduction of a quad-port cross-slot antenna with simultaneously co-polarized and dual-polarized patterns," *IEEE Transactions on Antennas and Propagation*, Vol. 72, No. 2, 1140–1149, Feb. 2024.

[11] Zeain, M. Y., M. Abu, A. A. Althuwayb, H. Alsariera, A. J. A. Al-Gburi, A. A. Abdulbari, and Z. Zakaria, "A new technique of FSS-based novel chair-shaped compact MIMO antenna to enhance the gain for sub-6 GHz 5G applications," *IEEE Access*, Vol. 12, 49 489–49 507, 2024.

[12] Mondal, P., D. Dhara, and A. R. Harish, "A partially reflective fss-based superstrate as a decoupling structure for reducing the mutual coupling of circularly polarized antennas," *IEEE Transactions on Antennas and Propagation*, Vol. 72, No. 4, 3652–3661, Apr. 2024.

[13] Yan, S., Q. Chen, X. Guo, Z. Qiao, Q. Yang, S. Feng, Z. Huang, L. Yang, and Y. Li, "A high-isolation high-gain MIMO millimeter-wave antenna array," *IEEE Transactions on Antennas and Propagation*, Vol. 72, No. 2, 1201–1211, Feb. 2024.

[14] Devana, V. N. K. R., A. Beno, C. P. Devadoss, Y. Sukanya, C. V. R. Sankar, P. Balamuralikrishna, S. Chandrasekhar, and K. V. Babu, "A compact self isolated MIMO UWB antenna with band notched characteristics," *IETE Journal of Research*, 1–12, Feb. 2024.

[15] Kudumu, V. P. and V. S. P. Mokkapati, "A slot-shaped EBG structure for improving the isolation between patch arrays," *International Journal of Microwave & Optical Technology*, Vol. 15, No. 3, 2020.

[16] Kamal, S. and P. Sen, "Microstrip-ministered proximity-coupled stacked dual-port antenna for 6G applications," *IEEE Access*, Vol. 12, 2817–2829, Jan. 2024.

[17] Peng, X. and C. Du, "A flexible CPW-fed tri-band four-port MIMO antenna for 5G/WIFI 6E wearable applications," *AEU — International Journal of Electronics and Communications*, Vol. 174, 155036, 2024.

[18] Sharma, U., G. Srivastava, M. K. Khandelwal, and R. Roges, "Design challenges and solutions of multiband MIMO antenna for 5G/6G wireless applications: A comprehensive review," *Progress In Electromagnetics Research B*, Vol. 104, 69–89, 2024.

[19] Malathi, A. C. J., B. V. K. Reddy, and K. R. Phanindra, "A decoupling method using split ring resonator (SRR) for tri-band MIMO antenna for WLAN LTE band and 5G applications," *AEM Journal*, Vol. 13, No. 1, 19–24, Apr. 2024.

[20] Devana, V. N. K. R., A. Beno, C. P. Devadoss, Y. Sukanya, C. V. R. Sankar, P. Balamuralikrishna, S. Chandrasekhar, and K. V. Babu, "A compact self isolated MIMO UWB antenna with band notched characteristics," *IETE Journal of Research*, 1–12, Feb. 2024.

[21] Nadeem, I. and D.-Y. Choi, "Study on mutual coupling reduction technique for MIMO antennas," *IEEE Access*, Vol. 7, 563–586, 2018.

[22] Madni, A., M. R. Akram, K. Riaz, H. U. Rahman, M. U. Rehman, W. T. Khan, and M. Q. Mehmood, "A compact high isolation wideband MIMO antenna for multi-band applications," *Journal of Electromagnetic Waves and Applications*, Vol. 36, No. 14, 2041–2054, Mar. 2022.

[23] Nej, S., A. Ghosh, S. Ahmad, J. Kumar, A. Ghaffar, and M. I. Hussein, "Design and characterization of 10-elements MIMO antenna with improved isolation and radiation characteristics for mm-Wave 5G applications," *IEEE Access*, Vol. 10, 125 086–125 101, 2022.

[24] Elsharkawy, R. R., K. F. A. Hussein, and A. E. Farahat, "Dual-band (28/38 GHz) compact MIMO antenna system for millimeter-wave applications," *Journal of Infrared, Millimeter, and Terahertz Waves*, Vol. 44, No. 11, 1016–1037, Oct. 2023.

[25] Ali, W. A. E., A. A. Ibrahim, and A. E. Ahmed, "Dual-band millimeter wave 2 × 2 MIMO slot antenna with low mutual coupling for 5G networks," *Wireless Personal Communications*, Vol. 129, No. 4, 2959–2976, Mar. 2023.

[26] Sufian, M. A., N. Hussain, A. Abbas, J. Lee, S. G. Park, and N. Kim, "Mutual coupling reduction of a circularly polarized MIMO antenna using parasitic elements and DGS for V2X communications," *IEEE Access*, Vol. 10, 56 388–56 400, 2022.

[27] Najafy, V. and M. Bemani, "Mutual-coupling reduction in triple-band MIMO antennas for WLAN using CSRRs," *International Journal of Microwave and Wireless Technologies*, Vol. 12, No. 8, 762–768, Mar. 2020.

[28] Prasad, K. V. and M. V. Prasad, "Mutual coupling reduction between slotted-T MIMO elements for UWB applications," *Progress In Electromagnetics Research C*, Vol. 107, 203–217, 2021.

[29] Nimmagadda, S. M., S. Penke, V. K. Padarti, S. Vanka, and S. N. M. Nemalikanti, "Design of an edge-truncated patch antenna (ETPA) for near-range vehicular RADAR applications," *AIP Advances*, Vol. 14, No. 1, 015326, 2024.

[30] Varzakas, P., "Average channel capacity for Rayleigh fading spread spectrum MIMO systems," *International Journal of Communication Systems*, Vol. 19, No. 10, 1081–1087, Dec. 2006.